UDC 624.04
IRSTI 67.03
RESEARCH ARTICLE

THE MULLER-BRESLAU ACTIVE EARTH PRESSURE COEFFICIENT: VALIDITY DOMAIN AND QUANTIFICATION OF THE PLANAR FAILURE-SURFACE ERROR

A. Aniskin[1], K. Moskalova[1], M. Oreskovic[1], Sh.Zh. Zharassov[2*]

[1]University North, 42000, Varazdin, Croatia
[2]L.N. Gumilyov Eurasian National University, 010000, Astana, Kazakhstan

Abstract. *The Müller-Breslau closed-form solution for the active earth pressure coefficient Ka(φ, α, β, δ) remains the standard design tool for cohesionless backfill, yet its parameter domain is documented only fragmentarily and the error of its planar failure-surface assumption is rarely isolated from other sources of discrepancy between calculation methods. This study maps the admissible domain over the practical range of soil friction angles, φ = 20-45°, and wall inclinations α = -20° to +20° and quantifies the planar-surface error in a unified computational framework. Direct numerical maximization of the Coulomb trial wedge, formulated with the admissibility conditions ρ ≤ 90° + α and R ≥ 0, reproduces the closed form to within 0.015% over 8 970 parameter combinations, so that the difference from Sokolovski's method of characteristics measures the planar failure-surface error alone. This error is governed primarily by the wall inclination rather than by wall friction: its median does not exceed about 1% for vertical walls and for α = +10° but reaches 6.6-16% at α = -20°, locally above 30%, consistently on the unsafe side - a finding verified independently by a rotational log-spiral upper-bound mechanism. The results are condensed into applicability maps dividing the parameter space into safe, caution and significant-error zones, and a step-by-step design procedure with a worked example shows how the maps are used to decide whether the closed form may be applied directly or must be replaced by a rigorous solution.*

Keywords: *active earth pressure; Müller-Breslau formula; Coulomb wedge; method of characteristics; retaining wall; limit equilibrium.*

***Corresponding author**
Shyngys Zharassov, e-mail: zhshzh95@gmail.com

https://doi.org/10.51488/1680-080X/2026.3-12

ӘОЖ 624.04
ҒТАМР 67.03
ҒЫЛЫМИ МАҚАЛА

МЮЛЛЕР-БРЕСЛАУ БЕЛСЕНДІ ТОПЫРАҚ ҚЫСЫМЫНЫҢ КОЭФФИЦИЕНТІ: ҚОЛДАНЫЛУ АЙМАҒЫ ЖӘНЕ ЖАЗЫҚ СЫРҒАНАУ БЕТІНІҢ ҚАТЕЛІГІН САНДЫҚ БАҒАЛАУ

А. Анискин[1], К. Москалова[1], М. Орешкович[1], Ш.Ж. Жарасов[2]*

[1]Солтүстік Университеті, 42000, Вараждин, Хорватия
[2]Л.Н.Гумилев атындағы Еуразия ұлттық университеті, 010000, Астана, Қазақстан

Аңдатпа. *Мюллер-Бреслаудың жердің белсенді қысым коэффициентіне арналған жабық түрдегі ерітіндісі Ka (φ, α, β, δ) когезиясыз толтыруды жобалаудың стандартты құралы болып қала береді, дегенмен оның параметрлік домені тек фрагменттік түрде құжатталған және оның қателігі жазықтықтың істен шығуы-беттік болжам есептеу әдістері арасындағы сәйкессіздіктің басқа көздерінен сирек оқшауланған. Бұл зерттеу топырақтың үйкеліс бұрыштарының практикалық диапазонындағы рұқсат етілген доменді, φ = 20-45° және қабырғалардың α = -20°-тан +20° - қа дейінгі бейімділіктерін картаға түсіреді және жазықтық-беттік қатені бірыңғай есептеу жүйесінде сандық түрде анықтайды. Рұқсат етілген шарттармен тұжырымдалған Кулондық сынақ сынасының тікелей сандық максимизациясы ρ ≤ 90° + α және R ≥ 0, жабық пішінді 8 970 параметр комбинациясынан 0,015% шегінде көбейтеді, Осылайша Соколовскийдің сипаттамалар әдісінен айырмашылығы тек жазықтықтағы ақаулық-беттік қатені өлшейді. Бұл қате, ең алдымен, қабырғаның үйкелісіне емес, қабырғаның көлбеуіне байланысты: оның медианасы тік қабырғалар үшін шамамен 1%-дан аспайды және α = +10°, бірақ α = -20° кезінде 6,6 - 16%-ға жетеді, жергілікті деңгейде 30%-дан жоғары, тұрақты түрде қауіпті жағында-бұл нәтиже айналмалы журнал-спираль тәрізді жоғарғы шекара механизмімен тәуелсіз тексеріледі. Нәтижелер параметр кеңістігін қауіпсіз, сақтық және елеулі қателіктер аймақтарына бөлетін қолдану карталарына жинақталады және жұмыс істеп тұрған мысалмен қадамдық жобалау процедурасы карталардың жабық пішінді тікелей қолдануға болатынын немесе қажет екенін шешу үшін қалай пайдаланылатынын көрсетеді. қатаң шешіммен ауыстырылады.*

Түйінді сөздер: *белсенді топырақ қысымы; Мюллер-Бреслау формуласы; Кулон сынасы; сипаттамалар әдісі; тіреу қабырғасы; шектік тепе-теңдік.*

***Автор-корреспондент**
Шынгыс Жарасов, e-mail: zhshzh95@gmail.com

https://doi.org/10.51488/1680-080X/2026.3-12

УДК 624.04
МРНТИ 67.03
НАУЧНАЯ СТАТЬЯ

КОЭФФИЦИЕНТ АКТИВНОГО ДАВЛЕНИЯ ГРУНТА МЮЛЛЕРА-БРЕСЛАУ: ОБЛАСТЬ ПРИМЕНИМОСТИ И КОЛИЧЕСТВЕННАЯ ОЦЕНКА ПОГРЕШНОСТИ ПЛОСКОЙ ПОВЕРХНОСТИ СКОЛЬЖЕНИЯ

А. Анискин[1], К. Москалова[1], М. Орешкович[1], Ш.Ж. Жарасов[2]*

[1]Университет Север, 42000, Вараждин, Хорватия
[2]Евразийский национальный университет имени Л.Н. Гумилева, 010000, Астана, Казахстан

Аннотация. *Замкнутое решение Мюллера-Бреслау для определения коэффициента активного давления на грунт Ka(φ, α, β, δ) остается стандартным инструментом проектирования безнапорной засыпки, однако область его параметров задокументирована лишь фрагментарно, а ошибка, связанная с предположением о плоской поверхности разрушения, редко изолируется от других источников расхождений между ними. Методы расчета. Это исследование отображает допустимую область в практическом диапазоне углов трения о грунт φ = 20-45° и наклонов стен α = от -20° до +20° и количественно определяет погрешность плоской поверхности в единой вычислительной системе. Прямая численная максимизация кулоновского пробного клина, разработанного с учетом условий допустимости ρ ≤ 90° + α и R ≥ 0, воспроизводит замкнутую форму с точностью до 0,015% для 8 970 комбинаций параметров, так что отличие от метода характеристик Соколовского измеряется только погрешностью плоской поверхности разрушения. Эта погрешность определяется в первую очередь наклоном стены, а не ее трением: ее среднее значение не превышает примерно 1% для вертикальных стен и при α = +10°, но достигает 6,6-16% при α = -20°, локально превышает 30%, постоянно на небезопасной стороне - подтвержденный результат независимо друг от друга с помощью вращающегося бревенчато-спирального механизма верхнего переплета. Результаты сведены в карты применимости, разделяющие пространство параметров на зоны безопасности, осторожности и зоны со значительными ошибками, а пошаговая процедура проектирования с проработанным примером показывает, как эти карты используются для принятия решения о том, может ли закрытая форма применяться непосредственно или должна быть заменена строгим решением.*

Ключевые слова: *активное давление грунта; формула Мюллера-Бреслау; клин Кулона; метод характеристик; подпорная стена; предельное равновесие.*

***Автор-корреспондент**
Шынгыс Жарасов, e-mail: zhshzh95@gmail.com

https://doi.org/10.51488/1680-080X/2026.3-12

1 INTRODUCTION

The determination of active earth pressure on retaining structures is one of the oldest problems of soil mechanics, and the wedge solution of Coulomb [1] remains its most influential formulation. Its generalization to an inclined wall, sloping backfills and wall friction, given in closed form by Müller-Breslau [2], is today the standard design tool for cohesionless backfill and is embedded, in identical or lightly modified form, in Eurocode 7 and in numerous national standards. The formula expresses the active earth pressure coefficient K_a as an explicit function of four angles - the soil friction angle φ, the wall inclination α, the backfill slope β and the wall friction angle δ - obtained analytically from the stationarity condition of the thrust with respect to the inclination ρ of a planar trial failure surface.

Two distinct questions accompany any closed-form limit-equilibrium solution: over what parameter domain is the expression valid, and how large is the error introduced by its mechanical idealization? For the Müller-Breslau formula, both questions have been answered only fragmentarily. Individual algebraic restrictions - such as the requirement $\beta \leq \varphi$ for the radicand to remain non-negative – are stated in textbooks [3-4] but a systematic mapping of the complete admissible domain in (α, β, δ) space, distinguishing algebraic boundaries, degenerate mechanisms and mechanical limits, is to the authors' knowledge not available. The practical need for such a map is real: design situations combining steep backfill, inclined walls and high interface friction routinely approach the domain boundaries, where the formula remains formally computable while the underlying wedge mechanism degenerates. Beyond its research value, such a map has a didactic purpose: it allows both experienced engineers and students to see at a glance where the closed-form solution is safe, where it degrades, and why - reducing the risk of misapplication near the domain boundaries.

The second question - the error of the planar failure-surface assumption - has a long history. Rigorous reference solutions for earth pressure are provided by the method of characteristics of Sokolovski [5], whose tabulated values remain a benchmark and whose framework continues to be applied to earth pressure problems [6], and by the tables of Caquot and Kérisel [7] and Kérisel and Absi [8] based on log-spiral surfaces. The slip-line framework has since been extended and systematized for retaining-wall problems: critical slip fields for both limit states [9], general wall inclination and backfill slope [10], a rigorous treatment of the boundary-value structures of the solution [11], c-φ and seismic condition [6;12], axisymmetric and circular wall geometries [3;14] and specific wall kinematics and arching effects [15,16]. Within the framework of limit analysis [17], kinematic (upper-bound) solutions with rotational log-spiral mechanisms [18-19] and static (lower-bound) stress fields [20-21] bracket the exact collapse load, and modern finite-element limit analysis provides tight numerical bounds for arbitrary geometries [22]. From these comparisons it is generally accepted that the planar assumption is benign for the active case, in contrast to the passive case, where Coulomb-type solutions may overestimate resistance drastically for large wall friction [8;17]. However, published comparisons typically report differences between complete computational chains – different numerical methods, discretization's and sign conventions - so that the contribution of the planar surface itself is not cleanly isolated from other sources of discrepancy.

The present paper addresses both questions in a unified computational framework. First, the admissible domain of the Müller-Breslau formula is mapped over the practical range of soil friction angles, $\varphi = 20–45°$, covering the full physical ranges of α, β and δ. Second, the closed form is verified against direct numerical maximization of the Coulomb trial wedge, formulated as a wedge-equilibrium problem with two unknown force magnitudes, subject to two admissibility conditions that are seldom stated explicitly: the geometric cap $\rho \leq 90° + \alpha$ on the trial-plane inclination, and the compression requirement $R \geq 0$ on the slip-plane reaction, without which non-physical solutions arise near the singular direction $\rho = \alpha + \delta + \varphi - 90°$, where the wall and slip-plane reactions become parallel. The agreement of the closed form with the numerical optimum to within 0.015% establishes that the two are computationally interchangeable; consequently, the difference between the Müller-Breslau solution and the method of characteristics is a pure measure of the planar failure-surface error. This error is then quantified over the whole parameter space using a slip-line solver validated against

https://doi.org/10.51488/1680-080X/2026.3-12

Sokolovski's published tables and cross-checked by an independent rotational log-spiral upper-bound mechanism [17;19], and the results are condensed into practical applicability maps that divide the parameter space into a region of safe application, a region of significant planar-surface error, and the mathematically inadmissible exterior. All results can additionally be explored through interactive web applications provided as supplementary material [23-24].

2 MATERIALS AND METHODS

2.1 The Müller-Breslau closed form and sign conventions

The geometry and sign conventions used throughout this paper are defined in Figure 1.

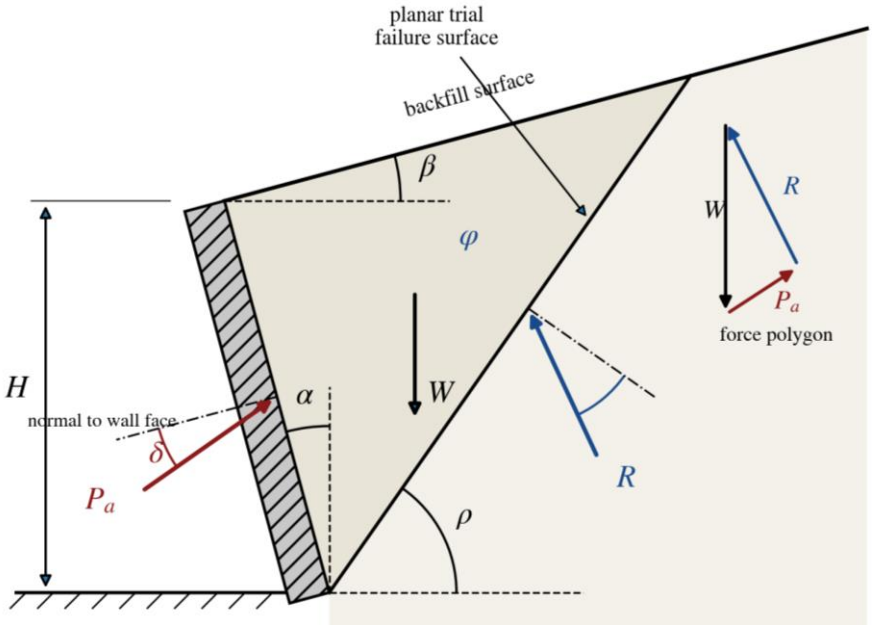

Figure 1 – Definition of the geometry, sign conventions and forces of the Coulomb trial-wedge problem. All angles are shown in their positive directions; the trial-plane inclination ρ is measured from the horizontal at the wall heel, with the admissible range φ < ρ < 90° + α [Author's material]

The wall face is inclined at α to the vertical (positive when the soil rests on the inclined face), the backfill surface at β to the horizontal (positive upward away from the wall), and the wall friction angle δ is positive when the soil settles relative to the wall. The active earth pressure coefficient is given by Müller-Breslau [2] as:

$$K_a = \frac{cos^2(\varphi-\alpha)}{cos^2\alpha\cos(\alpha+\delta)\left[1+\sqrt{\frac{sin(\varphi+\delta)sin(\varphi-\beta)}{\cos(\alpha+\delta)\cos(\alpha-\beta)}}\right]^2} \quad (1)$$

and defines the total active thrust per unit length of wall,

$$P_a = \frac{1}{2}K_\alpha \gamma \mathrm{H}^2 \quad (2)$$

where γ is the unit weight of the backfill and H the vertical height of the wall; the factor $\cos^2\alpha$ in the denominator of (1) accounts for the increased length of the inclined face. The thrust acts at the angle δ to the normal of the wall face, so that its line of action is inclined at (α + δ) to the horizontal and the horizontal and vertical components follow as

$$P_h = P_a cos(\alpha + \delta),\ P_v = P_a sin(\alpha + \delta) \quad (3)$$

https://doi.org/10.51488/1680-080X/2026.3-12

For $\alpha = 0$ these reduce to the familiar $\cos\delta$ and $\sin\delta$ decomposition; for inclined walls the use of $\cos\delta$ alone is a common source of error, as is the confusion between Ka and the horizontal coefficient $K_{ah} = K_a \cdot \cos(\alpha + \delta)$ tabulated by some references. Expression (1) is real-valued only for $\beta \le \varphi$ and $\delta \ge -\varphi$, with the additional requirements $\alpha + \delta < 90°$ and $|\alpha - \beta| < 90°$ for the cosines in the denominator to remain positive; these algebraic boundaries are examined in the Results and Discussion.

2.2 Direct numerical optimization of the Coulomb wedge

Independently of (1), the active thrust was computed by direct numerical maximization of the Coulomb trial-wedge problem. For a planar trial surface inclined at ρ to the horizontal and passing through the wall heel (Figure 1), the equilibrium of the wedge under its weight W, the re-action R on the slip plane (inclined at φ to the plane's normal) and the reaction of the wall (inclined at δ to the face normal) yields the thrust $E(\rho)$ in closed form from the force polygon; the active thrust is $P_a = \max E(\rho)$. Two admissibility conditions, seldom stated explicitly in the literature, are essential for robust numerical treatment. First, the trial-plane inclination is geometrically capped by the wall face itself, $\varphi < \rho < 90° + \alpha$, the upper bound corresponding to the trial plane coinciding with the wall face itself, at which the wedge enclosed between the two degenerates to zero area and the thrust vanishes. Second, the reaction on the slip plane must be compressive, $R \ge 0$: near the singular direction $\rho = \alpha + \delta + \varphi - 90°$, at which the wall and slip-plane reactions become parallel, the force polygon degenerates and unconstrained equilibrium admit non-physical solutions with tensile R. With both conditions imposed, the maximization was carried out by golden-section search refined to $|\Delta\rho| < 10^{-6}$ rad on a dense grid over the full parameter space.

2.3 Reference solution: method of characteristics

Rigorous reference values were computed with a slip-line solver implementing Sokolovski's method of characteristics for a cohesionless soil with self-weight [5]. The governing hyperbolic system is integrated along with the two families of characteristics inclined at $\pm(45° - \varphi/2)$ to the direction of the major principal stress, marching from the stress boundary condition on the backfill sur-face toward the wall. Depending on the parameter combination, the solution takes one of three structures (Figure 2): (A) a continuous field integrated by marching along the characteristics from the known stress state on the backfill surface toward the wall, with the free parameter iteratively adjusted until the wall friction condition is satisfied (a shooting procedure); (B) a solution containing a stress discontinuity; or (C) a degenerate single-zone (Rankine-type) field when the wall condition is fully consistent with the surface condition. The solver was validated against Sokolovski's published tables: of 99 tabulated values spanning $\varphi = 10 - 40°$, 88 were reproduced within the adopted tolerance, with a maximum deviation of 2.2% (Table 1). The mobilized wall friction is capped at the value consistent with the characteristic field ($\delta_{mob} \le \delta$), and cells at which this cap is active are flagged.

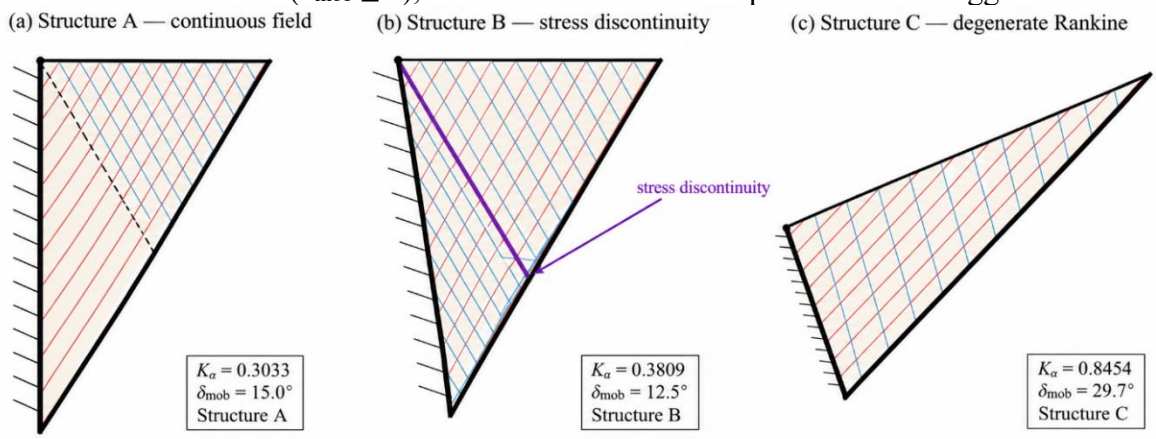

Figure 2 – The three structures of the slip-line field for the active case (examples for $\varphi = 30°$): (a) continuous field (structure A; $\alpha = 0°$, $\beta = 0°$, $\delta = 15°$); (b) field containing a stress discontinuity (structure B; $\alpha = +10°$, $\beta = 0°$, $\delta = 12.5°$); (c) degenerate single-zone Rankine-type field (structure C; $\alpha = +20°$, $\beta = 22.5°$, $\delta = 30°$). Both characteristic families are shown; the bold line marks the outermost slip surface [Author's material]

https://doi.org/10.51488/1680-080X/2026.3-12

2.4 Independent verification: rotational log-spiral upper bound

As an independent cross-check of the characteristic's solution, the active thrust was additionally bounded by a rotational log-spiral mechanism in the framework of the kinematic theorem of limit analysis [17;19]. A rigid region bounded by the wall face, the backfill surface and a log-spiral slip surface through the wall heel rotates about a center whose two coordinates are the optimization variables; the spiral pitch equals tan φ, so that the velocity jump is inclined at φ to the surface and, for a cohesionless soil, no internal energy is dissipated. The thrust follows from the balance of the work rates of gravity and of the wall reaction, assumed to act at the lower third of the face at the angle δ to its normal, and is maximized over the position of the rotation center. Since the planar wedge is the limiting member of this family as the center recedes to infinity, the mechanism yields values $K_{a,LS} \geq K_{a,MB}$, while the kinematic theorem guarantees $K_{a,LS} \leq K_{a,exact}$ for the active problem; the mechanism therefore brackets the exact coefficient from below and provides a one-sided check on the characteristics solution that does not depend on its implementation. The implementation was verified to reproduce the Rankine value $K_a = \tan^2(45° - \varphi/2)$ to five digits in the smooth-vertical-wall limit.

2.5 Parametric grid and classification of the planar-surface error

The parametric grid covers φ ∈ {20, 25, 30, 35, 40, 45}°, α ∈ {-20, -10, 0, +10, +20}°, β from -25° to φ - 2.5° in steps of 2.5°, and δ from 0 to φ in steps of φ/12 - in total 8 970 combinations, of which 8 705 yielded a converged characteristic solution. The count follows directly from the grid construction: for each of the six values of φ, δ takes 13 values, while the number of backfill slopes grows with φ (18 to 28 values, since the admissible range β ≤ φ widens); over the five wall inclinations this gives 5 × 13 × (18 + 20 + 22 + 24 + 26 + 28) = 8 970. Of the 265 non-converged cells, 260 correspond to backfill slopes at or beyond the natural stability limit of a cohesionless slope, |β| ≥ φ, and are therefore physically inadmissible regardless of the calculation method - notably, the Müller-Breslau expression remains real-valued there, since its radicand restricts only β ≤ φ and not β ≥ −φ; only 5 cells (0.06% of the grid) represent genuine non-convergence of the characteristics solver, all at the corner δ = φ. The lower bound of the friction-angle range reflects the practical limit for genuinely cohesionless soils: effective friction angles below about 20° are essentially confined to cohesive or organic materials outside the c = 0 framework [4]. For each cell the relative difference $\Delta = (K_{a,SOK} - K_{a,MB})/K_{a,MB}$ is evaluated and the parameter space is classified into three zones: zone A, |Δ| < 2%, in which the planar-surface error is below the practical uncertainty of determining φ itself; zone B, 2% ≤ |Δ| < 5%, comparable to the margins implied by partial safety factors; and zone C, |Δ| ≥ 5%, in which the planar assumption produces a significant and - since Δ > 0 predominates - unconservative error. Interactive web applications through which the complete parameter space can be explored are provided as supplementary material.

3 RESULTS AND DISCUSSION

3.1 Equivalence of the closed form and the numerical wedge optimum

Over all 8 970 grid combinations spanning φ = 20-45°, the closed-form expression (1) and the direct numerical maximization of the trial wedge described in the Methodology agree to within 0.015% (maximum relative deviation 0.0143%, median 0.0005%) (Figure 3). No parameter combination was found within the physical domain at which the stationary point of the thrust falls outside the admissible range φ < ρ < 90° + α; the closed form and the constrained numerical optimum are therefore computationally interchangeable, and the breakdown of the Müller-Breslau solution occurs exclusively at the domain boundaries, not inside the domain. This equivalence is the key that unlocks the remainder of the paper: since the closed form is an exact evaluation of the planar-wedge model, any difference between it and a rigorous solution measures the planar-surface assumption alone. The behavior of K_a over the (β, δ) plane for successive wall inclinations is shown in Figure 3, and the assembled three-parameter function $K_a(\alpha, \beta, \delta)$ in Figure 5.

https://doi.org/10.51488/1680-080X/2026.3-12

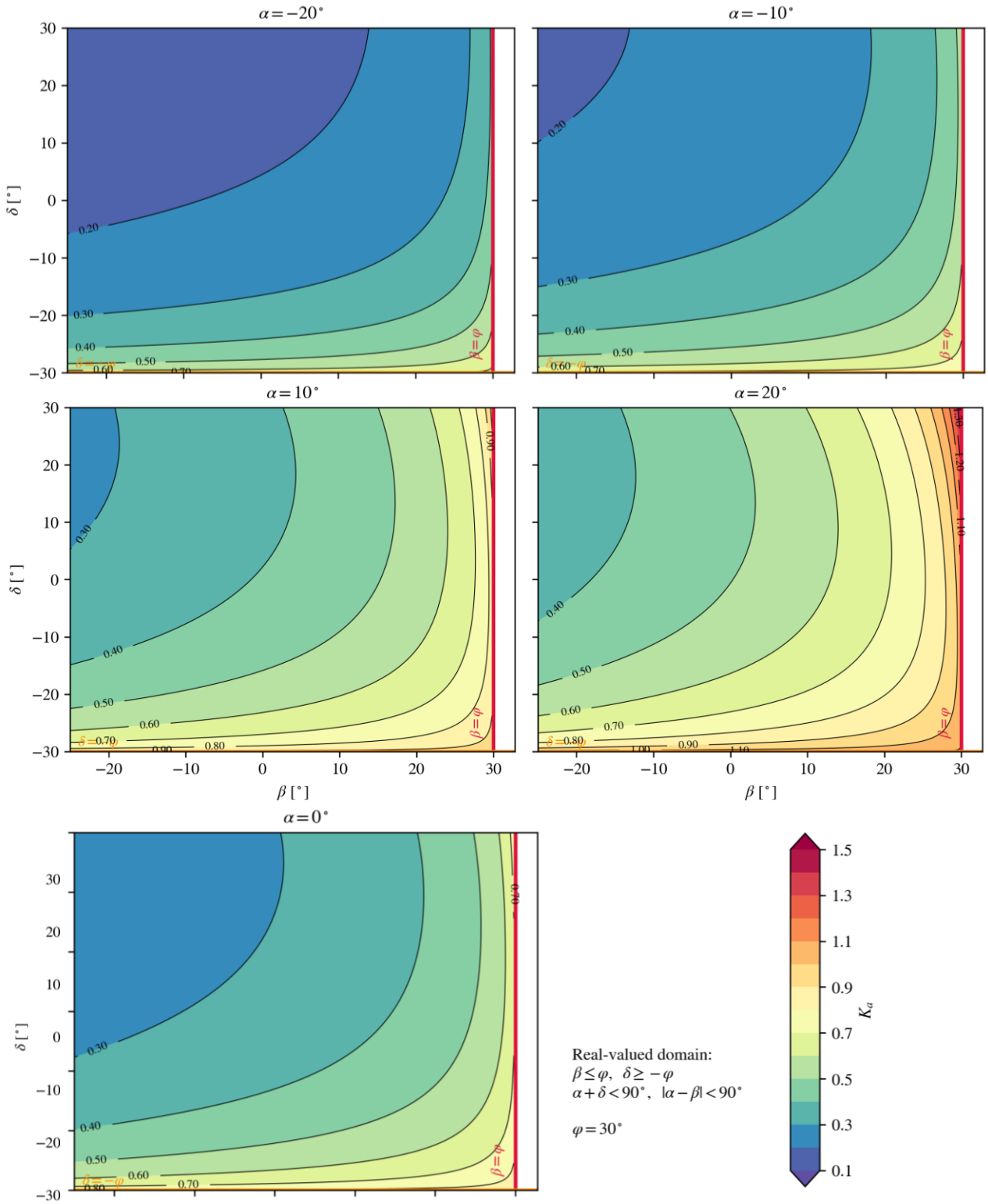

Figure 3 – Müller–Breslau coefficient $K_a(\beta, \delta)$ at constant wall inclination α (example shown for φ = 30°), with the algebraic boundaries β = φ and δ = −φ marked [Author's material]

3.2 Critical failure-plane angle and the degenerate limit β approaching φ

Figure 4 maps the critical plane inclination ρcr(β, δ). As β approaches φ the critical plane rotates toward the backfill surface, ρ_{cr} tends to β, and the sliding wedge grows without bound while K_a itself remains finite.

https://doi.org/10.51488/1680-080X/2026.3-12

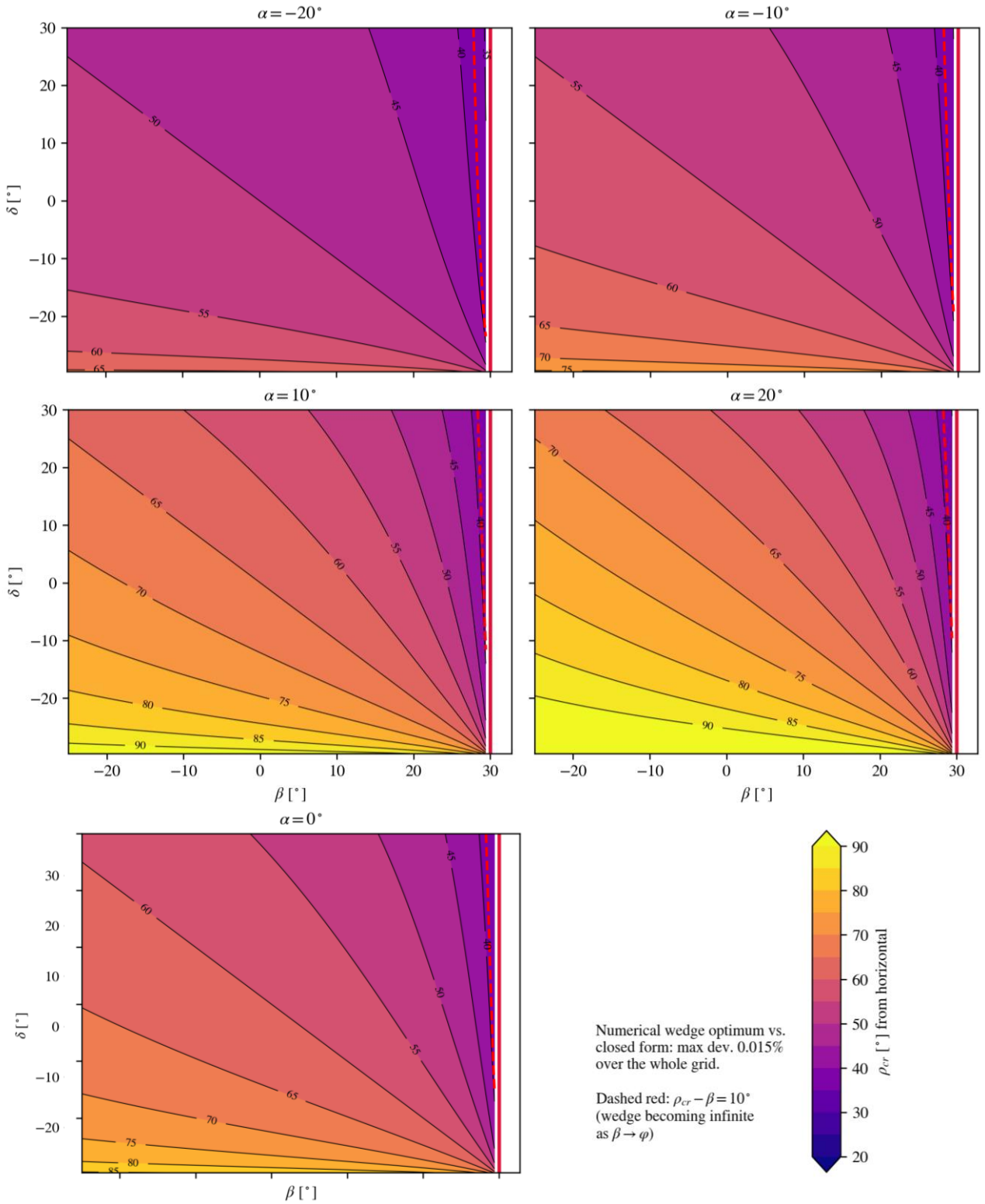

Figure 4 – Critical failure-plane inclination $\rho_{cr}(\beta, \delta)$ of the Coulomb wedge for wall inclinations α = −20°, −10°, 0°, +10° and +20° (example shown for φ = 30°); the dashed red line marks the contour $\rho_{cr} - \beta = 10°$, indicating proximity to the degenerate limit β → φ [Author's material]

The contour ρ_{cr} - β = 10°, marked in Figure 4, provides a practical proximity indicator to this degenerate limit: beyond it, small uncertainties in β or φ translate into large changes of the mechanism geometry. A second numerically important feature is the singular direction ρ = α + δ + φ − 90°, at which the wall and slip-plane reactions become parallel and the unconstrained force polygon admits

https://doi.org/10.51488/1680-080X/2026.3-12

non-physical equilibrium states with tensile slip-plane reaction; with the constraint R ≥ 0 imposed, these states are excluded and the optimization remains stable throughout the domain.

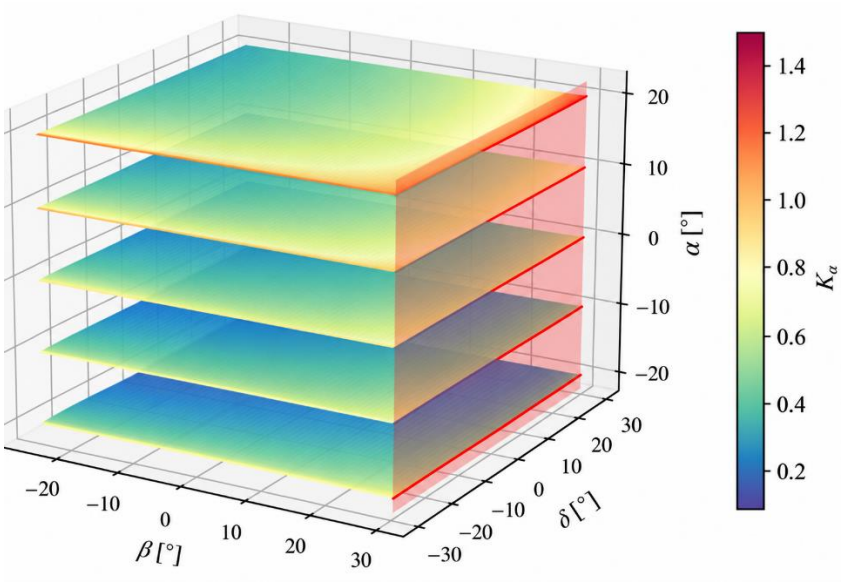

Figure 5 – Stacked-slice visualization of the three-parameter function $K_a(\alpha, \beta, \delta)$ at constant φ; the red plane marks the boundary β = φ [Author's material]

3.3 Validation of the characteristic's solver

Table 1 summarizes the validation of the slip-line solver against Sokolovski's published tables. Of 99 tabulated values spanning φ = 10-40°, 88 are reproduced within the adopted tolerance, with a maximum deviation of 2.2%; the exceptions concentrate at φ = 10°, where the tabulated values are published to two significant digits only, so that the residual deviations reflect primarily the rounding and the coarse computational grids of the original tables rather than the accuracy of the present solver.

Table 1 – Validation of the slip-line solver against Sokolovski's tabulated active-pressure values [Author's material] / [5]

№	φ [°]	cells	within tolerance	max deviation [%]
1	10	27	19	2.19
2	20	24	24	1.07
3	30	27	24	2.06
4	40	21	21	2.23
Total		99	88	2.23

3.4 Planar-surface error across the parameter space

Table 2 gives the median of the relative difference $\Delta = (K_{a,SOK} - K_{a,MB})/K_{a,MB}$ over the (β, δ) plane for each combination of φ and α; the median - the value exceeded in exactly half of the grid cells - is reported because the distribution of Δ is strongly skewed by the near-boundary tail, which is characterized separately by the 90th percentile and the maximum; Figure 7a plots the same data. Two observations organize the entire error landscape. First, the difference is positive in 98.7% of all cells: the method of characteristics yields the larger coefficient, so the planar assumption errs on the unsafe side for active pressure. Second - and contrary to the common textbook emphasis on wall friction - the governing parameter is the wall inclination α, not δ. For vertical walls and α = +10° the median error remains between about 0.5% and 1% for all φ, fully consistent with the received view that the planar assumption is benign in the active case. For negatively inclined walls the picture changes qualitatively: at α = -10° the median rises to 2.6-4.3%, and at α = −20° to 6.6% (φ = 20°) up to 16.0% (φ = 45°), with 90th percentiles above 20% and local values up to 35%. For α = +20° a secondary growth appears at high φ (median 4.2% at φ = 45°), together with a small region near δ = φ as β

https://doi.org/10.51488/1680-080X/2026.3-12

approaches φ in which the sign reverses and the Müller-Breslau value exceeds the rigorous one (by up to 2% at φ = 30°, growing to 9% at φ = 45°) - the only conservative corner of the domain.

The distribution of the solution structures across the grid is itself informative: of the 8 705 converged cells, 5 971 exhibit the continuous field (structure A), 2 701 contain a stress discontinuity (structure B), and only 33 degenerates to the single Rankine-type zone (structure C; Figure 2). These cells are confined to the corner of positive wall inclination with fully mobilized wall friction (α ≥ +10°, δ = φ, β approaches φ), and they correspond one-to-one with the only region in which the sign of the planar-surface error reverses: every cell with Δ < -0.2% is of structure C, and every structure-C cell has Δ ≤ 0. Where the characteristic field collapses to a single Rankine-type zone, the Müller-Breslau solution slightly overestimates the rigorous coefficient - the only conservative corner of the domain.

Table 2 – Median relative difference Δ [%] between the method of characteristics and the Müller-Breslau solution [Author's material]

№	φ [°]	α = -20°	α = -10°	α = 0°	α = +10°	α = +20°
1	20	6.56	2.64	0.93	0.49	0.53
2	25	8.18	3.08	1.04	0.54	0.67
3	30	9.42	3.42	0.96	0.54	0.94
4	35	10.87	3.53	0.88	0.54	1.64
5	40	12.91	3.84	0.77	0.60	2.67
6	45	15.96	4.33	0.68	0.82	4.19

3.5 Independent verification by the rotational log-spiral bound

Because the largest differences occur in a corner of the domain where any single numerical method might be suspected of degradation, the characteristics solution was cross-checked with the independent rotational log-spiral upper-bound mechanism described in the Methodology. Table 3 reports the three methods at representative points. The kinematic bound brackets the result from below in every case, and the sandwich $K_{a,MB} \leq K_{a,LS} \leq K_{a,SOK}$ closes to within 0.2–2%: at the most extreme verified point (φ = 30°, α = −20°, β = −25°, δ = 20°), the log-spiral mechanism alone already requires a coefficient 17.4% above the Müller-Breslau value, against 17.6% from the method of characteristics. The large planar-surface error at negative wall inclinations is therefore established by two independent methods and cannot be attributed to solver artifacts.

Table 3 – Three-method comparison at representative points: Müller-Breslau (planar mechanism), rotational log-spiral upper-bound mechanism (LS), and method of characteristics (SOK) [Author's material]

№	φ [°]	α [°]	β [°]	δ [°]	$K_{a,MB}$	$K_{a,LS}$	$K_{a,SOK}$	(LS−MB)/MB [%]	(SOK−MB)/MB [%]
1	20	0	0	10	0.4467	0.4490	0.4494	+0.51	+0.59
2	20	−20	−10	10	0.2969	0.3260	0.3264	+9.82	+9.97
3	30	0	0	15	0.3014	0.3030	0.3033	+0.54	+0.62
4	30	−10	−10	15	0.2164	0.2271	0.2275	+4.94	+5.14
5	30	−20	−25	20	0.1454	0.1707	0.1711	+17.38	+17.63
6	30	−20	−25	30	0.1388	0.1680	0.1711	+21.08	+23.31
7	40	0	0	20	0.1994	0.2004	0.2005	+0.50	+0.57
8	40	−10	0	20	0.1400	0.1459	0.1465	+4.20	+4.58
9	45	0	0	22.5	0.1597	0.1604	0.1605	+0.46	+0.53

3.6 Applicability maps

The findings are condensed into the applicability maps of Figure 6, which classify the (β, δ) plane for each wall inclination into the safe-application zone A (|Δ| < 2%, below the practical uncertainty of φ itself), the caution zone B (2-5%), and zone C (|Δ| ≥ 5%), with the mathematically inadmissible exterior marked separately.

https://doi.org/10.51488/1680-080X/2026.3-12

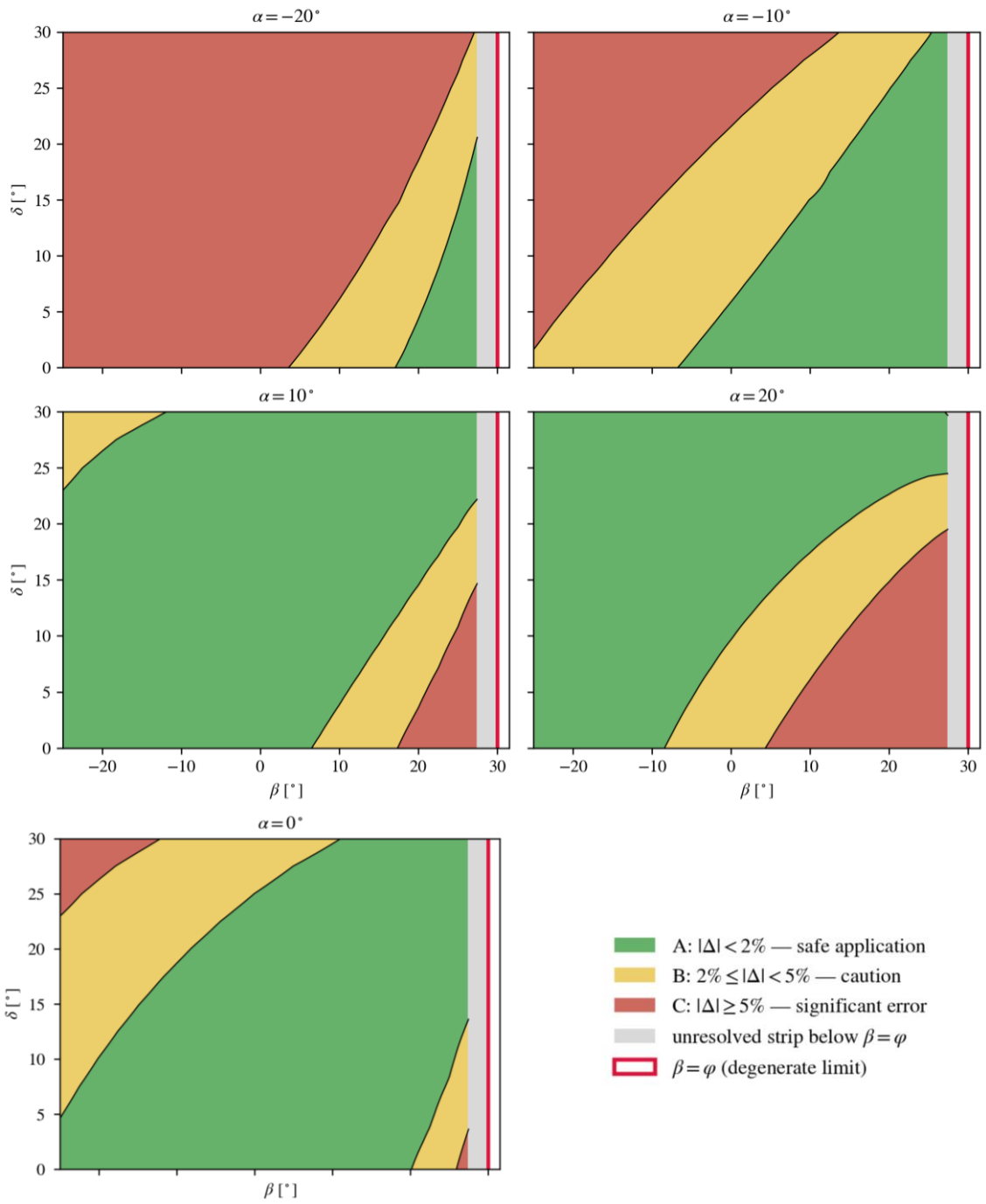

Figure 6 – Applicability map of the Müller–Breslau formula (example shown for φ = 30°): zone A (|Δ| < 2%), zone B (2–5%), zone C (≥5%); grey – unresolved band between the last grid cell and β = φ; crimson line – degenerate limit β = φ. Isolated non-converged cells (5 of 8 970 over all φ) were infilled from neighboring cells for display [Author's material]

Figure 7b summarizes the zone-A share across all φ. For vertical walls zone A occupies 68-78% of the physically admissible (β, δ) grid cells, depending on φ, and for α = +10° up to 84%; zone C is confined to the strip adjoining the degenerate limit as β approaches φ. For α = −20°, in contrast, the safe zone shrinks to between 15% (φ = 20°) and below 1% (φ = 45°), and zone C occupies most of the plane regardless of δ. The practical reading is im-mediate: the Müller-Breslau formula may be used without correction for near-vertical and positively inclined walls away from the narrow band of the parameter plane adjacent to the degenerate limit β = φ, while for negatively inclined walls a rigorous method - or at minimum a log-spiral correction - is required for any friction angle.

https://doi.org/10.51488/1680-080X/2026.3-12

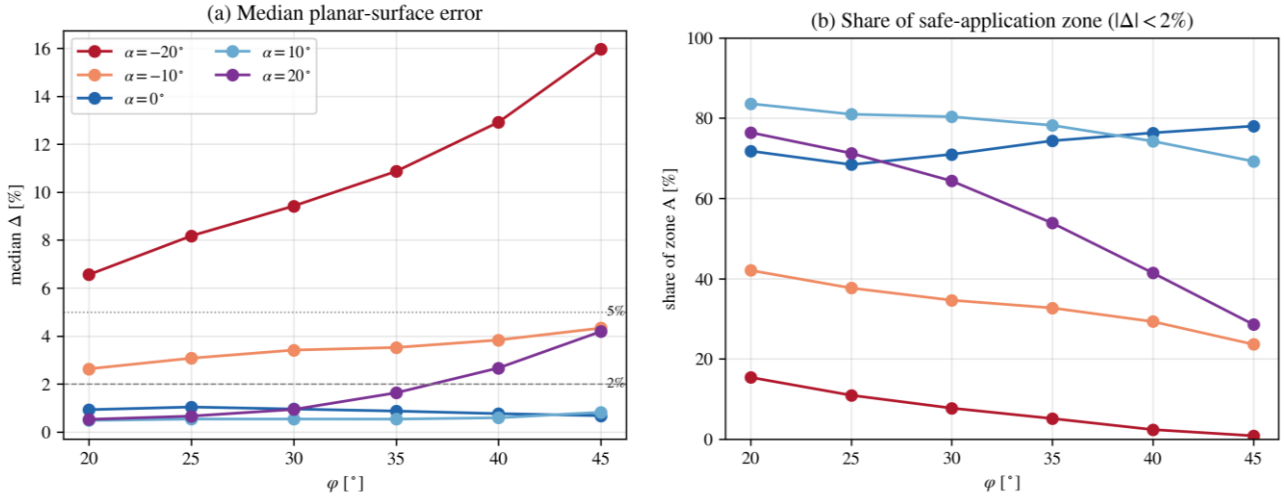

Figure 7 – Summary over the friction-angle range: (a) median planar-surface error and (b) share of the safe-application zone A, as functions of φ for each wall inclination α [Author's material]

The results admit a transparent interpretation in the framework of the limit theorems [17]. The Coulomb wedge is the simplest kinematic mechanism for the active problem, and its exact evaluation - the Müller-Breslau closed form - is consequently a mechanism-based estimate that approaches the true coefficient from below; the method of characteristics constructs a stress field consistent with the yield condition and, when extensible, approaches it from above the mechanism estimates. The empirical sandwich $K_{a,MB} \leq K_{a,LS} \leq K_{a,SOK}$ observed at every verified point of Table 3 is exactly the ordering the theorems predict, and the narrow gap between the rotational bound and the characteristics solution (0.2–2%) indicates that both are close to the exact value. Within this picture, the 0.015% agreement between the closed form and the constrained numerical wedge is not a new mechanical result but an essential verification: it certifies that the entire difference reported in Tables 2-3 belongs to the failure-surface geometry and not to the algebra or the numeric of the wedge model [23-26].

The dominance of the wall inclination α over the wall friction δ has a simple geometric explanation. For a vertical or positively inclined wall, the critical planar surface is short and the true (curved) slip surface deviates from it only mildly, so the classical view that the active case is insensitive to the planar assumption is confirmed - and now quantified at 0.5-1.0% median over the full (β, δ) plane. For a negatively inclined wall the wedge is compressed between an overhanging face and the backfill: the critical plane steepens, the singular direction $\rho = \alpha + \delta + \varphi - 90°$ approaches the admissible range, and the true slip surface acquires pronounced curvature to satisfy the boundary condition on the face. The planar surface can no longer follow, and its error grows with both |α| and φ. Notably, the error remains substantial at δ = 0 in this regime - wall friction merely modulates a discrepancy created by the wall geometry.

The practical implications are direct. On the unsafe side, the planar assumption may understate the active thrust on negatively inclined walls by 10-30% in realistic parameter ranges; such geometries arise, for example, in gravity walls with inclined rear faces, in the equivalent-wall idealizations of some composite systems, and in rock-cut support with adverse face orientation. For these cases the applicability maps of Figure 5 give an immediate screening tool, and a characteristic, log-spiral or finite-element limit analysis solution [22] should replace the closed form whenever the point of interest falls outside zone A. Conversely, for most conventional configurations - near-vertical walls with β safely below φ - the maps justify the continued use of the Müller-Breslau formula with quantified confidence, which is itself a conclusion of direct practical value, even if an expected one. The small conservative pocket at α = +20°, δ = φ, β approaches φ is of theoretical rather than practical interest, but it demonstrates that the sign of the planar-surface error is not universal.

Two numerical by-products deserve emphasis because they affect anyone re-implementing the wedge optimization, including in teaching. Without the geometric cap $\rho \leq 90° + \alpha$ the optimizer can

https://doi.org/10.51488/1680-080X/2026.3-12

wander into wedges that intersect the wall, and without the compression condition $R \geq 0$ it can converge to false stationary points near the singular direction where the wall and slip-plane reactions are parallel; both failure modes produce plausible-looking but meaningless coefficients. Neither condition is stated in the standard derivations [2;4], and both were encountered in the present computations before being controlled. In relation to the slip-line literature, the present contribution is complementary to the systematic treatment of the boundary-value structures by Peng and Chen [11]: their focus is the correct construction of the rigorous solution, whereas here the rigorous solution is used as a reference against which the closed-form planar model is calibrated and mapped.

The study is limited to a dry, homogeneous, cohesionless backfill under static conditions, to resultant forces rather than pressure distributions, to the associated flow rule implicit in both limit analysis and the method of characteristics, and to wall inclinations $|\alpha| \leq 20°$. The extension to cohesive backfill via the theorem of corresponding states is exact only for smooth walls, so the present error maps cannot simply be transformed to c-φ soil; the seismic extension through the Mononobe-Okabe formula, which is the Müller-Breslau solution under rotated gravity, suggests that the α-governed error structure identified here transfers directly to the seismic case, where the effective wall inclination is modified by the seismic angle [21] - both extensions are left for future work, as is the passive case, where the planar-surface error is known to be far more sever [8;19]. Consequently, the error maps apply to cohesionless backfill ($c' = 0$) only; for cohesive backfill a method accounting for cohesion must be used and extending the present comparison to c'–φ' soils, for which slip-line solutions are available [12], is the first priority of future work, as it would considerably widen the practical scope of the results.

3.7 Procedure for practical use and worked example

The results of this study are applied in design by the following sequence (Figure 8).

Step 1 - Establish the input data: the effective friction angle φ and unit weight γ of the back-fill, the vertical height H and inclination α of the wall, the backfill slope β and the design wall friction angle δ.

Step 2 - Check admissibility: $\beta \leq \varphi$, $|\beta| < \varphi$, $0 \leq \delta \leq \varphi$, $\alpha + \delta < 90°$ and $|\alpha - \beta| < 90°$; outside these limits expression (1) must not be used.

Step 3 - Check the proximity to the degenerate limit (Figure 4): if $\rho_{cr} - \beta < 10°$, small uncertainties in β or φ strongly change the failure mechanism, and a rigorous solution is recommended.

Step 4 - Compute $K_{a,MB}$ from expression (1).

Step 5 - Locate the point (β, δ) on the applicability map for the given α (Figure 6 for φ = 30°; the interactive tools provided as supplementary material for other φ) and read the zone and the local value of Δ.

Step 6 - In zone A use $K_{a,MB}$ directly; in zone B use the corrected value $K_a = K_{a,MB}\cdot(1 + \Delta)$ or a rigorous solution; in zone C replace expression (1) by the method of characteristics, a log-spiral mechanism or finite-element limit analysis.

Step 7 - Compute P_a, P_h and P_v from (2) and (3) and use them in the verification of the wall with the partial factors of the adopted Eurocode 7 design approach.

Worked example. A wall of vertical height H = 6 m retains a dry cohesionless backfill with $\gamma = 18$ kN/m³ and φ = 30°. Variant 1: vertical back face (α = 0°), horizontal backfill (β = 0°), δ = 15°. All admissibility conditions hold, $\rho_{cr} = 56.9°$ lies far from β, and (1) gives $K_{a,MB} = 0.3014$. The point lies in zone A (Δ = +0.62%, Table 3), so the closed form is used directly: $P_a = 0.5\cdot0.3014\cdot18\cdot6^2 = 97.7$ kN/m, $P_h = P_a\cdot\cos 15° = 94.3$ kN/m and $P_v = P_a\cdot\sin 15° = 25.3$ kN/m.

Variant 2: back face inclined at α = −20°, backfill sloping at β = −25°, δ = 20°. The admissibility conditions again hold ($\rho_{cr} = 50.4°$), and (1) gives $K_{a,MB} = 0.1454$, i.e. $P_a = 47.1$ kN/m. The point, however, lies in zone C (Δ = +17.6%, Table 3): the method of characteristics gives $K_{a,SOK} = 0.1711$, and the log-spiral bound alone already requires $K_{a,LS} = 0.1707$. The design thrust is therefore $P_a = 0.5\cdot0.1711\cdot18\cdot6^2 = 55.4$ kN/m, acting horizontally since α + δ = 0 ($P_h = P_a$, $P_v = 0$). Applying the

https://doi.org/10.51488/1680-080X/2026.3-12

closed form without the check of Step 5 would underestimate the active thrust by 8.3 kN/m, i.e. by about 15% of the rigorous value, before any partial factor is applied.

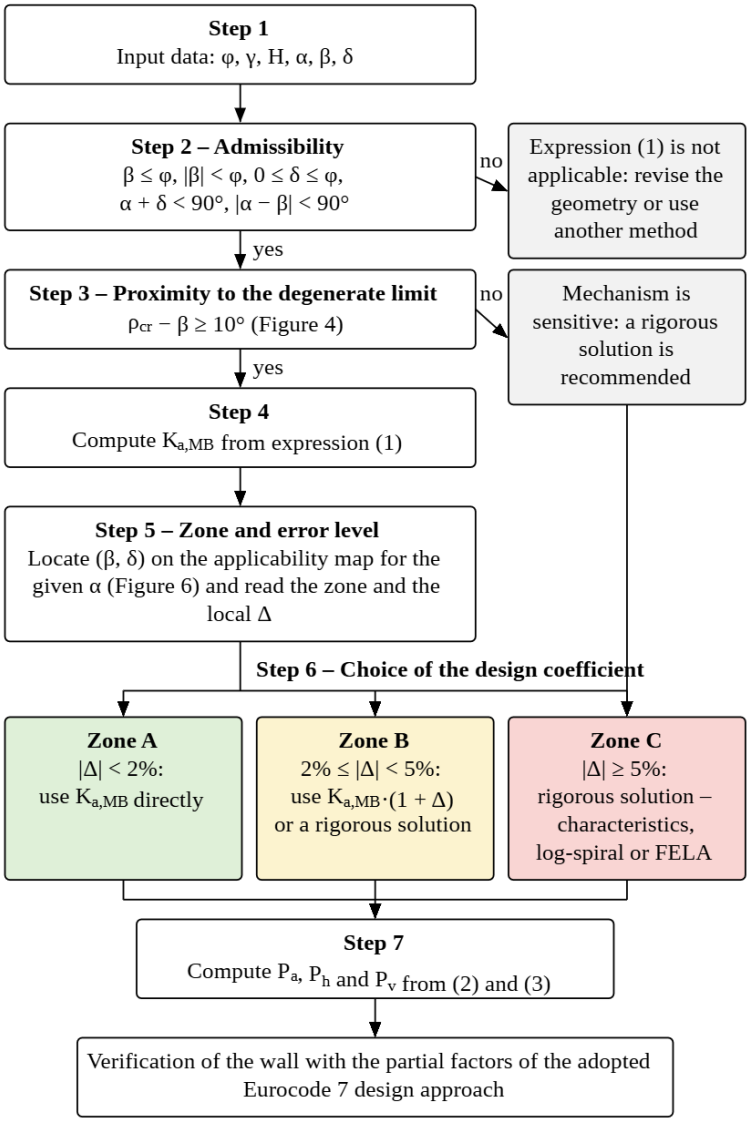

Figure 8 – Procedure for the practical use of the applicability maps: admissibility and proximity checks, zone identification and the corresponding choice of the active earth pressure coefficient [Author's material]

4 CONCLUSIONS

This paper mapped the validity domain of the Müller-Breslau active earth pressure coefficient and quantified the error of its planar failure-surface assumption over the practical parameter space φ = 20–45°, α = ±20°, β ≤ φ, 0 ≤ δ ≤ φ. The main findings are as follows.

1. Direct numerical maximization of the Coulomb trial wedge, with the admissibility conditions ρ ≤ 90° + α and R ≥ 0 imposed, reproduces the closed form to within 0.015% overall 8 970 parameter combinations; no interior region of inadmissible stationary points exists, and the difference between the Müller-Breslau solution and the method of characteristics is therefore a pure measure of the planar failure-surface error.

2. This error is governed primarily by the wall inclination α. For vertical walls and α = +10° its median is about 0.5-1% for all friction angles, confirming and quantifying the received view, while at α = +20° it grows to 4.2% at φ = 45°; for α = -10° it rises to 2.6-4.3%, and for α = −20° to 6.6–16.0%, with local values exceeding 30%, consistently on the unsafe side.

https://doi.org/10.51488/1680-080X/2026.3-12

3. The finding is confirmed independently by a rotational log-spiral upper-bound mechanism, which brackets the characteristics solution to within 0.2-2% at all verified points, so that the ordering Müller-Breslau ≤ log-spiral ≤ characteristics predicted by the limit theorems is observed throughout.

4. Applicability maps classify the parameter space into a safe-application zone ($|\Delta| < 2\%$; 68–84% of the physical plane for $\alpha \geq 0$, shrinking to below 1% for $\alpha = -20°$ at high φ), a caution zone (2-5%) and a significant-error zone (≥5%), and delineate the algebraic boundaries and the degenerate limit as β approaches φ, at which the formula remains finite while the wedge mechanism becomes unbounded.

5. For design practice, the Müller-Breslau formula may be used with quantified confidence for near-vertical walls away from the narrow band of the parameter plane adjacent to the degenerate limit $\beta = \varphi$, while negatively inclined walls require a rigorous solution for any wall friction; the interactive applications accompanying this paper allow both regimes to be explored directly.

6. A step-by-step procedure (Section 3.7) links the maps to design practice - admissibility check, proximity check $\rho_{cr} - \beta \geq 10°$, zone identification and, outside zone A, correction or replacement of the closed-form coefficient; the worked example shows that for a negatively inclined wall the closed form may underestimate the active thrust by about 15%. The maps are restricted to cohesionless backfill; their extension to cohesive soils is the subject of future work.

REFERENCES

1. **Coulomb, M.** (2023). Essai sur une application des règles de Maximis & Minimis à quelques Problèmes de Statique, relatifs à l'Architecture. Revue Française de Géotechnique, (175), 1. https://doi.org/10.1051/geotech/2023019
2. **Muller-Breslau, H. F. B.** (1906). Erddruck auf Stützmauern. A. Kröner. http://onlinebooks.library.upenn.edu/webbin/book/lookupid?key=ha002011844
3. **Clayton, C. R. I., Woods, R. I., Bond, A. J., & Milititsky, J.** (2014). Earth Pressure and Earth-Retaining Structures (3rd ed.). CRC Press. https://www.routledge.com/Earth-Pressure-and-Earth-Retaining-Structures/Clayton-Woods-Bond-Milititsky/p/book/9781466552111
4. **Terzaghi, K.** (1943). Theoretical Soil Mechanics (1st ed.). Wiley. https://doi.org/10.1002/9780470172766
5. **Sokolovskii, V. V.** (1965). Statics of Granular Media (J. K. Lusher, Trans.). Oxford: Pergamon Press. https://www.sciencedirect.com/book/9780080136240/statics-of-granular-media
6. **Santhoshkumar, G., & Ghosh, P.** (2018). Seismic passive earth pressure on an inclined cantilever retaining wall using method of stress characteristics – A new approach. Soil Dynamics and Earthquake Engineering, 107, 77–82. https://doi.org/10.1016/j.soildyn.2018.01.021
7. **Caquot, A. I., & Kérisel, J. L.** (1948). Tables for the Calculation of Passive Pressure, Active Pressure and Bearing Capacity of Foundations. Paris. https://www.scirp.org/reference/referencespapers?referenceid=3646522
8. **Kerisel, J., & Absi, E.** (2017). Active and Passive Earth Pressure Tables (3rd ed.). Routledge. https://doi.org/10.1201/9781315136615
9. **Zhu, D.-Y., Qian, Q.-H., & Lee, C. F.** (2001). Active and passive critical slip fields for cohesionless soils and calculation of lateral earth pressures. Géotechnique, 51(5), 407–423. https://doi.org/10.1680/geot.2001.51.5.407
10. **Liu, F. Q., & Wang, J. H.** (2008). A generalized slip line solution to the active earth pressure on circular retaining walls. Computers and Geotechnics, 35(2), 155–164. https://doi.org/10.1016/j.compgeo.2007.06.002
11. **Peng, M. X., & Chen, J.** (2013). Slip-line solution to active earth pressure on retaining walls. Géotechnique, 63(12), 1008–1019. https://doi.org/10.1680/geot.11.P.135
12. **Cheng, Y. M.** (2003). Seismic lateral earth pressure coefficients for c–φ soils by slip line method. Computers and Geotechnics, 30(8), 661–670. https://doi.org/10.1016/j.compgeo.2003.07.003

https://doi.org/10.51488/1680-080X/2026.3-12

13. **Cheng, Y. M., Hu, Y. Y., & Wei, W. B.** (2007). General Axisymmetric Active Earth Pressure by Method of Characteristics–Theory and Numerical Formulation. International Journal of Geomechanics, 7(1), 1–15. https://doi.org/10.1061/(ASCE)1532-3641(2007)7:1(1)
14. **Keshavarz, A., & Ebrahimi, M.** (2016). The Effects of the Soil-Wall Adhesion and Friction Angle on the Active Lateral Earth Pressure of Circular Retaining Walls. International Journal of Civil Engineering, 14(2), 97–105. https://doi.org/10.1007/s40999-016-0016-3
15. **Lin, Y., Chen, F., Yang, J., & Li, D.** (2020). Active Earth Pressure of Narrow Cohesionless Backfill on Inclined Rigid Retaining Walls Rotating about the Bottom. International Journal of Geomechanics, 20(7), 04020102. https://doi.org/10.1061/(ASCE)GM.1943-5622.0001727
16. **Paik, K. H., & Salgado, R.** (2003). Estimation of active earth pressure against rigid retaining walls considering arching effects. Géotechnique, 53(7), 643–653. https://doi.org/10.1680/geot.2003.53.7.643
17. **Chen, W. F.** (1975). Limit Analysis and Soil Plasticity. Developments in Geotechnical Engineering, Vol. 7. Amsterdam: Elsevier. https://www.sciencedirect.com/bookseries/developments-in-geotechnical-engineering/vol/7/suppl/C
18. **Chen, W. F., & Liu, X. L.** (1990). Limit Analysis in Soil Mechanics. Developments in Geotechnical Engineering, Vol. 52. Amsterdam: Elsevier. https://books.google.com/books/about/Limit_Analysis_in_Soil_Mechanics.html?id=rvFRAAAAMAAJ
19. **Soubra, A.-H., & Macuh, B.** (2002). Active and passive earth pressure coefficients by a kinematical approach. Proceedings of the Institution of Civil Engineers - Geotechnical Engineering, 155(2), 119–131. https://doi.org/10.1680/geng.2002.155.2.119
20. **Lancellotta, R.** (2002). Analytical solution of passive earth pressure. Géotechnique, 52(8), 617–619. https://doi.org/10.1680/geot.2002.52.8.617
21. **Mylonakis, G., Kloukinas, P., & Papantonopoulos, C.** (2007). An alternative to the Mononobe–Okabe equations for seismic earth pressures. Soil Dynamics and Earthquake Engineering, 27(10), 957–969. https://doi.org/10.1016/j.soildyn.2007.01.004
22. **Sloan, S. W.** (2013). Geotechnical stability analysis. Géotechnique, 63(7), 531–571. https://doi.org/10.1680/geot.12.RL.001
23. **Salauat, M. S., Aldigaziyeva, A. K., & Bashayeva, A. A.** (2025). Research on the effectiveness of using the rubber-soil method. Bulletin of the Kazakh Leading Academy of Architecture and Civil Engineering, 95(1), 197–206. https://doi.org/10.51488/1680-080X/2025.1-13
24. **Shadkam, A. S., Bessimbayev, E. T., Begaliev, U. T., & Niyetbay, S. E.** (2024). The comparison of deformation calculation results of structures under seismic impact using mohr-coulomb and hardening soil small (HSS) soil models. Bulletin of the Kazakh Leading Academy of Architecture and Civil Engineering, 94(4), 193–202. https://doi.org/10.51488/1680-080X/2024.4-16
25. **Surovtseva, N. V., Abakanov, T., & Nigmetov, G. M.** (2026). Experimental studies of the seismic vulnerability of a building model on strengthened soils. Bulletin of the Kazakh Leading Academy of Architecture and Civil Engineering, 99(1), 311–325. https://doi.org/10.51488/1680-080X/2026.1-21
26. **Tursynbayev, N. A., Abdrasilov, L., Yeleussinova, A. Y., Aubakirova, B. B., Tungyshbayeva, S. Zh., Yermekbayev, B. Zh., Sagin, J., & Moldabaeva, G. N.** (2026). Efficiency of clay soils reinforcement in construction. Bulletin of the Kazakh Leading Academy of Architecture and Civil Engineering, 99(1), 355–366. https://doi.org/10.51488/1680-080X/2026.1-24

https://doi.org/10.51488/1680-080X/2026.3-12

FUNDING

This research received no external funding.

CONFLICT OF INTEREST

The authors declare no conflict of interest.

DATA AVAILABILITY STATEMENT

The data supporting the findings of this study are available from the corresponding author upon reasonable request.
The datasets and interactive computational tools supporting this study are publicly available in Zenodo. The Müller–Breslau/Coulomb earth pressure coefficient visualization tool is available at https://zenodo.org/records/21473601, while the Sokolovski method-of-characteristics solver for active and passive earth pressure coefficients is available at https://zenodo.org/records/21474178.

ARTIFICIAL INTELLIGENCE STATEMENT

Claude (Anthropic; model Claude Fable 5, accessed July 2026) was used as an auxiliary tool for: preparation and cross-checking of numerical verification scripts (Coulomb-wedge optimization and a rotational log-spiral upper-bound mechanism), preparation of figures from the author's computed datasets, literature screening, and language editing. All computations of record were produced and validated with the author's own solvers; all methodological decisions, interpretations, conclusions and the final wording were made, verified and approved by the author.

AUTHOR CONTRIBUTIONS

Aleksej Aniskin – conceptualization, research supervision, methodology, critical revision of the manuscript.
Khrystyna Moskalova – collection and analysis of regulatory documents, validation, writing, review and editing.
Matija Orešković – research methodology, methodological guidance.
Shyngys Zharassov – visualization, formatting and technical editing of the manuscript.

INFORMATION ABOUT THE AUTHORS

- Aleksej Aniskin
- PhD, Assist. prof.
- University North
- Varazdin, Croatia
- E-mail address: aaniskin@unin.hr
- ORCID ID: https://orcid.org/0000-0002-9941-1947

- Khrystyna Moskalova
- PhD, Assist. prof.
- University North
- Varazdin, Croatia
- E-mail address: kmoskalova@unin.hr
- ORCID ID: https://orcid.org/0000-0002-2543-9154

https://doi.org/10.51488/1680-080X/2026.3-12

• Matija Oreškovic
• Assist. prof.
• University North
• Varazdin, Croatia
• E-mail address: moreskovic@unin.hr
• ORCID ID: https://orcid.org/0000-0001-5684-0496

• Shyngys Zharassov
• PhD., Senior Lecturer
• L.N. Gumilyov Eurasian National University
• Astana, Kazakhstan
• E-mail address: zhshzh95@gmail.com
• ORCID ID: https://orcid.org/0000-0002-0468-8362

Received: 25 July 2026
Revised: 15 August 2026
Accepted: 18 September 2026

https://doi.org/10.51488/1680-080X/2026.3-12